Water Resources Research

RESEARCH ARTICLE
10.1029/2018WR024251

Key Points:
- We propose a relative permeability model based on pore-scale flow regimes
- We identify the scaling of the normalized relative permeability and fractional flow
- We validate the proposed model against data collected from the literature

Correspondence to:
I. Battiato,
ibattiat@stanford.edu

Citation:
Picchi, D., & Battiato, I. (2019). Relative permeability scaling from pore-scale flow regimes. *Water Resources Research*, *55*. https://doi.org/10.1029/2018WR024251

Received 11 OCT 2018
Accepted 9 MAR 2019
Accepted article online 18 MAR 2019

Relative Permeability Scaling From Pore-Scale Flow Regimes

D. Picchi[1] and I. Battiato[1]

[1]Department of Energy Resources Engineering, Stanford University, Stanford, CA, USA

Abstract Relative permeability measurements are commonly fitted with the Corey and Brooks-Corey correlations. Despite such correlations fit experimental data generally well, they are mostly of an empirical nature. Here, we propose a semiempirical model to determine relative permeabilities of the wetting and the nonwetting phases in real 3-D porous media that accounts for pore-scale flow regimes. The starting point is the homogenization framework proposed by Picchi and Battiato (2018, https://doi.org/10.1029/2018WR023172), where the upscaling is conducted for different spatial distributions of the flowing phases in the capillary tube setting. First, we extend the approach to realistic media by allowing pore-scale flow regimes to coexist in a complex geometry while accounting for capillary and viscous limits in the dynamics. Then, we discuss the scaling behavior of normalized relative permeabilities in terms of the phases viscosity ratio and identify three classes which govern their scaling. We also derive an analytical expression for the fractional flow. Finally, we provide a detailed validation of the proposed model for both relative permeabilities and fractional flow against data from numerical simulations and experiments available in the literature. The data set used for validation covers a wide range of systems, ranging from brine-CO_2 to oil-water flows. The equations derived capture well the trend of both numerical and experimental data.

1. Introduction

The development of predictive tools to model multiphase flow through porous media is critical to many industrial applications, such as petroleum engineering (Lake, 1989), carbon sequestration (Yang et al., 2008), water resources, and modern energy storage technologies (Arunachalam et al., 2015). Although physical phenomena at the fine scale (i.e., the pore scale) may strongly affect phenomena on a vastly different scale (i.e., the continuum scale), macroscale (upscaled) models are routinely used to obtain predictions at the continuum scale in many practical applications, while pore-scale physics is taken into account only though averaged parameters.

The most common approach employed to model multiphase flows at the continuum scale is the two-phase Darcy's law, where the concept of relative permeabilities is introduced through empirical arguments (Bear, 1972; Leverett, 1941). Its structural resemblance with single-phase Darcy and its simplicity led to its widespread use, despite the abundant evidence from both experimental and theoretical analyses of its, often strong, limitations. Multiphase Darcy's law has been rigorously formulated by upscaling the Stoke's equation at the pore scale (e.g., Auriault, 1987; Daly & Roose, 2015; Hassanizadeh & Gray, 1980; Hornung, 1997; Lasseux et al., 2008; Kjelstrup et al., 2018; Whitaker, 1986), and since the microscopic details of the flow are usually neglected, its classical interpretation has been recently questioned. In fact, although the inherent instability of multiphase flows (Ling et al., 2017) may render the analysis of pore-scale distribution of the flowing phases challenging, recurring features in the topology of the nonwetting and wetting phase at the pore scale have been revealed by X-ray microtomography and high-performance computing (Armstrong et al., 2014, 2012, 2016; Blunt et al., 2013; Berg et al., 2013; Cueto-Felgueroso & Juanes, 2012; Gao et al., 2017; Garing et al., 2017; Li et al., 2005, 2018b; Lin et al., 2018; Prodanovic et al., 2006, 2007; Reynolds et al., 2017; Tallakstad et al., 2009; Tahmasebi et al., 2017; Zarikos et al., 2018). Experiments and simulations show that the nonwetting phase can become disconnected flowing in the form of individual ganglia or even remaining immobilized (trapped) in the porous matrix.

Specifically, Avraam and Payatakes (1995) classify the topology of the flowing phases at steady state into four possible pore-scale flow regimes: large ganglion dynamics, small ganglion dynamics, drop-traffic flow, and

connected pathway (CP) flow. Each flow regime differs from the others for the phase topology and phase connectivity: in the CP regime both phases flow through separate and uninterrupted pathways, while in large and small ganglion dynamics the nonwetting phase is disconnected and flows in the form of ganglia, much bigger (large ganglion) or smaller (small ganglion) than the average pore size. Furthermore, CP and ganglion dynamics flow regimes coexist in a wide range of conditions (Avraam & Payatakes, 1995; Armstrong et al., 2016; Gao et al., 2017): embedding such underlying physics becomes critical in developing more predictive macroscale models. For example, the nonuniqueness of closure relationships (e.g., the hysteric behavior of the relative permeability curves) has been associated with the transition from one regime to another (see Datta et al., 2014; Rucker et al., 2015; Schluter et al., 2016) and it is recognized as one of the main deficiencies of classical upscaled models.

Several approaches have been developed to incorporate the evolution of the fluid-fluid interface into macroscopic equations (e.g., Cueto-Felgueroso & Juanes, 2014; Gray & Miller, 2010; Gray et al., 2015; Hassanizadeh & Gray, 1990, 1993; Hilfer, 1998; Jackson et al., 2009; McClure et al., 2016; Niessner & Hassanizadeh, 2008; Rybak et al., 2015), but additional complexity in the formulation of the closure problem and in the definition of state variables has been inevitably introduced. Only recently, Karadimitriou et al. (2014) proposed a method to estimate such state variables from experimental measurements, while Schluter et al. (2016) and McClure et al. (2018) provided alternative approaches to identify the missing variables in terms of integral geometry (i.e., Euler characteristics). Over the years, more practical and ad hoc formulations of the relative permeabilities have been proposed (Chierici, 1984; Clavier et al., 2017; Dehghanpour et al., 2011; Gunstensen & Rothman, 1993; Li et al., 2018; Oliveira & Demond, 2003; Pasquier et al., 2017; Yiotis et al., 2007; Zhang et al., 2018), including the study of the impact of spatial heterogeneity on relative permeabilities (Jackson et al., 2018). To the best of our knowledge, a general formulation that accounts for the phase topology at the pore-scale of a 3-D porous medium has not been proposed yet.

More recently, Picchi and Battiato (2018) have proposed a new homogenization framework that allows one to derive upscaled equations that are regime specific: the main advantage of such an approach lies in incorporating the interactions between the flowing phases and the solid while retaining the simplicity of the final upscaled formulation. Specifically, the complexity of the problem is reduced by proposing an analogy between the flow regimes in real porous media and in a capillary tube, where the effective parameters of the macroscopic equations are determined by postulating the pore-scale flow regimes. As a result, although the geometry of the flowing phases has been simplified, the pore-scale physics of the interaction between different phases is retained and relative permeabilities of both the wetting and nonwetting phases have been analytically derived for CP, and small and large ganglion dynamics flow regimes. Although this approach is successful in quantifying the impact of flow regimes on relative permeabilities, it is limited to highly idealized configurations and its extension to complex porous media for relative permeability predictions dubious. Importantly, the question of whether or not any type of correction needs to be introduced in the context of a realistic porous media remains still open.

In this paper, we first propose a generalization of the homogenization approach proposed by Picchi and Battiato (2018) to realistic porous media, and, then, we validate our results against numerical and experimental data of two-phase flow available in the literature. Specifically, we propose a semiempirical formulation of the relative permeabilities that links the flow features in an idealized geometry (i.e., the capillary tube setting) to flow in a complex medium. The paper is organized as follows. In section 2 we obtain a generalized formulation for the relative permeability and the fractional flow by classifying real systems into three classes depending on the viscosity ratio. We discuss in details how pore-scale physics has been incorporated into the relative permeabilities, which depend only on the mobile phase saturation, the viscosity ratio, and the capillary number. In section 3, we first validate the model with data of pore-scale numerical simulations and, then, we test many experimental data available in the literature: the data cover a range in the capillary number and viscosity ratio of 7 and 2 orders of magnitude, respectively. The model provides the scaling of a normalized relative permeability of the wetting and nonwetting phases for all three classes. The analytical expressions of the fractional flow are also validated against experimental data in section 3.3. We provide summarizing comments in section 4.

2. Theoretical Considerations

In this section we propose a semiempirical generalization of the relative permeabilities developed in Picchi and Battiato (2018) to account for pore-scale flow regimes in complex porous media. For completeness and clarity, we first briefly review some of the results derived by Picchi and Battiato (2018, section 2.1) and, then, we present its generalization to model complex porous media (sections 2.2 and 2.3).

2.1. Relative Permeability Based on Pore-Scale Flow Regimes in a Capillary Tube

In this section we only briefly outline the results by Picchi and Battiato (2018) specifically used in this study. We refer to the original manuscript for further details. The fundamental premise of the framework proposed in Picchi and Battiato (2018) is that accurate estimates of relative permeabilities should explicitly account for the pore-scale topology of the flowing phases, i.e., for dynamic flow regimes, which control pore-scale connectivity. The upscaled equations developed allow one to account for CP, and large and small ganglion dynamics, where the closure relationships employed are regime specific and the macroscale equations are applicable to both viscous and inertial flow of two immiscible fluids in a porous medium. To make further analytical progress, the former regimes are associated to different flow patterns in capillary tubes, where flow in a bundle of capillaries, core-annular flow (CAF), and plug flow in a capillary are used as a dynamical analogs of the CP, large and small ganglion dynamics, respectively. We emphasize that *this analogy is based on the hypothesis that the most relevant features of the momentum transfer between phases could be captured at the leading order by their interactions in simplified settings (i.e., a capillary).* It is worth emphasizing that, while the analytical closures have been derived from well-known solutions of flow in capillaries, more sophisticated closures could be employed, if desired. The general model reduces to Darcy's law when (i) the contribution of inertia is negligible, i.e., at low Reynolds numbers; (ii) the driving force is the same for both phases; (iii) Eotvos number is small at the pore scale: this condition is often satisfied in real rocks where the characteristic length scale of the pores is sufficiently small to consider microgravity conditions. Since most of the data available in the literature and used in this study are collected at low Reynolds and Eotvos numbers, here we report results in the Darcy's limit only (see Picchi & Battiato, 2018, for a complete set of equations), i.e.,

$$\langle \overline{\boldsymbol{u}}_w \rangle = -\frac{k_w}{32} \nabla p_w, \tag{1a}$$

$$\langle \overline{\boldsymbol{u}}_{nw} \rangle = -\frac{k_{nw}}{32M} \nabla p_{nw}, \tag{1b}$$

where $\langle \overline{\boldsymbol{u}}_w \rangle$, $\langle \overline{\boldsymbol{u}}_{nw} \rangle$, k_w , k_{nw}, p_w, and p_{nw} are the average velocity, the relative permeabilities, and the macroscopic pressures of the wetting and the nonwetting phases, respectively, and $\langle \cdot \rangle$ is the average over a representative volume, while $\bar{\cdot}$ is the temporal average over a representative time interval. The viscosity ratio M is defined as

$$M = \frac{\mu_{nw}}{\mu_w}, \tag{2}$$

where μ_w and μ_{nw} are the dynamic viscosities of the wetting phase and the nonwetting phase, respectively. The dependence on pore-scale flow regimes is embedded in the relative permeabilities since they are directly affected by the spatial distribution and connectivity of the flowing phases. For the capillary tube analogy, they can be analytically expressed through one-dimensional closures relationships (Picchi et al., 2017, 2018; Ullmann & Brauner, 2004) for the *quasi-static* CP and the CAF regimes (Picchi & Battiato, 2018). Specifically, the CP regime can be conceptualized as a bundle of capillary tubes, see Figure 1a (right), and leads to the following relative permeability-saturation relationship

$$k_{w,\mathrm{CP}} = S_w^2, \qquad k_{nw,\ \mathrm{CP}} = (1 - S_w)^2. \tag{3}$$

For the CAF regime, see Figure 1c (right), one obtains

$$k_{w,\mathrm{CAF}} = S_w^2, \qquad k_{nw,\ \mathrm{CAF}} = (1 - S_w)^2 \left(1 + \frac{2MS_w}{1 - S_w}\right). \tag{4}$$

Equation (4), similar to those available in the literature (Dehghanpour et al., 2011), can be recovered as a particular case of more general relationships valid in the inertial regime and not discussed here—for more details see, for example, equation (26) in Picchi and Battiato (2018).

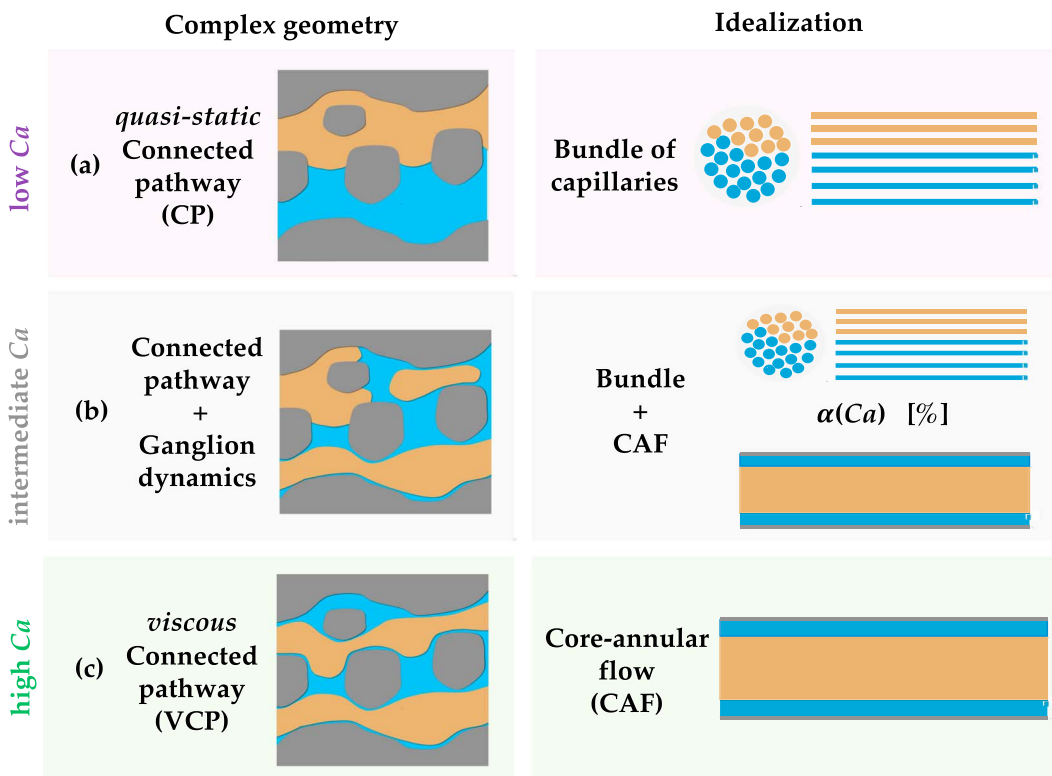

Figure 1. Sketch of flow regimes in a realistic geometry and their idealization in the framework of the capillary tube analogy. The wetting phase (light blue) and the nonwetting phase (dark orange) are referred in the text with the subscripts w and nw, respectively.

2.2. Generalization of Relative Permeabilities to Realistic Porous Media

In this section, we propose a generalization of the previous results to 3-D media with complex structures that accounts for residual fluid saturations, endpoint relative permeability different from unity, and the coexistence of flow regimes in the pore-domain.

The guiding principle of the analysis is the emerging evidence that the topological characteristics of the flow at the pore-scale change with the capillary number, defined as the ratio between viscous and capillary forces,

$$Ca = \frac{\mu_w U}{\sigma}, \tag{5}$$

where U is a velocity scale and σ is surface tension. The analysis of Armstrong et al. (2016) suggests that, at low capillary number, the flow is quasi-static (i.e., the fluid-fluid interface behaves like a rigid partition), while, at increasing capillary numbers, the volume fraction associated with connected ganglia, as well as the phases connectivity, increases due to coalescence of individual ganglia. Quoting from Armstrong et al. (2016),

> *"when Ca is increased (at constant S_w) the non-wetting phase clusters become longer and larger, forming tubes that enhance connectivity. The fluid arrangements observed at high Ca would be impossible at lower flow rates, where capillary forces dominate and drive the non-wetting phase to larger pores where the surface energy is minimized, i.e., non-wetting-phase becomes more spherical."*

Additionally, it has been observed, both in experiments and pore-scale numerical simulations (Armstrong et al., 2016; Avraam & Payatakes, 1995; Gao et al., 2017), that the transition away from the quasi-static regime takes place gradually and multiple flow regimes (i.e., CP and ganglion dynamics) coexist in a wide range of conditions.

In the proposed framework, we relate topological changes (i.e., phase connectivity) to the magnitude of the capillary number. Specifically,

- at low Ca (capillary limit), the flow is dominated by capillary forces and both phases flow through separate and uninterrupted pathways. Although regions of disconnected nonwetting phase may exist, the flowing phases advance mainly through preferential paths within which each phase is connected and wets the solid walls. We refer to this case as quasi-static CP flow regime; see Figure 1a.
- At intermediate Ca, a progressive mobilization of the nonwetting phase occurs through the onset of small and large ganglia; see Figure 1b. Coalescence and snap-off events, typical of ganglia flow, take place until the transition to the viscous regime is completed.
- At high Ca (viscous limit), viscous forces stabilize topological characteristics (Armstrong et al., 2016) by increasing the phases connectivity, namely, coalescence phenomena lead to the formation of very long ganglia. These long ganglia or *"tubes of nonwetting phase"* (quoting from Armstrong et al., 2016) are surrounded by a lubricating thin layer of the wetting phase, which covers the pore walls (Avraam & Payatakes, 1995). We refer to this regime as *viscous* connected pathway (VCP) flow, and we model it in analogy with the CAF regime; see Figure 1c. Although an idealization, CAF can quite realistically capture interactions between phases since the pore space is occupied by elongated ganglia and the key role of the wetting film is not neglected. As shown by Picchi et al. (2018), the CAF analogy is able to capture the physics of elongated bubbles.

Furthermore, in order to parametrize the transition from the capillary to the viscous limit at the Darcy scale, we introduce $\alpha \in (0, 1)$, here referred to as the flow regime parameter. The flow regime parameter, which accounts for the spatial heterogeneity of the flow regimes, represents the volumetric fraction of the medium occupied by VCP flow and can be written as

$$\alpha = f(Ca, \text{properties of the medium}). \tag{6}$$

We hypothesize that the transition from the capillary to the viscous limits varies linearly with the percentage of the whole core occupied by each flow regime, i.e. the relative permeability at a given intermediate capillary number is determined as a linear combination of the relative permeabilities in the quasi-static CP and the CAF regimes, with $1 - \alpha$ and α as the weighing functions, that is,

$$k_w\left(S_w, Ca\right) = (1-\alpha)\, k_{w,\mathrm{CP}} + \alpha k_{w,\mathrm{CAF}}, \tag{7a}$$

$$k_{nw}\left(S_w, M, Ca\right) = (1-\alpha) k_{nw,\mathrm{CP}} + \alpha k_{nw,\mathrm{CAF}}, \tag{7b}$$

where $k_{i,\mathrm{CP}}$ and $k_{i,\mathrm{CAF}}$, $i = \{w, nw\}$ are defined in equations (3) and (4). The validity of such a hypothesis will be tested in the following through direct comparison with data. The coexistence of ganglia and CP flow is controlled by the magnitude of the flow regime parameter ($0 \le \alpha \le 1$): when α is low, most of the fluid domain is occupied by CP flow with a small amount of disconnected ganglia, while for α close to 1, the pore space is mostly occupied by long and connected ganglia, i.e., relative permeabilities in equation (7) converge to k_{CP} and k_{CAF} for $\alpha = 0$ and $\alpha = 1$, respectively.

The idealization of flow regimes in a capillary tube, however, cannot account for trapping mechanisms during drainage or imbibition, i.e., for endpoint relative permeabilities different from one and/or irreducible and residual saturations. Therefore, we introduce a normalized relative permeability, k_w^*, and mobile saturation of the wetting phase, S_*, defined as

$$k_w^* = \frac{k_w}{\beta_w}, \qquad k_{nw}^* = \frac{k_{nw}}{\beta_{nw}}, \tag{8}$$

and

$$S_* = \frac{S_w - S_{ir}}{1 - S_{ir} - S_{or}}, \tag{9}$$

where β_w, β_{nw}, S_{ir}, and S_{or} are the endpoint relative permeability of the wetting and nonwetting phases, the irreducible saturation of the wetting phase and the residual saturation of the nonwetting phase, respectively. Combining equations (7), (8) and (9), we obtain the following expressions for the normalized relative permeabilities,

$$k_w^* = S_*^2, \tag{10a}$$

$$k_{nw}^{*} = \left(1 - S_{*}\right)^{2}\left(1 + \frac{2S_{*}}{1 - S_{*}}M\alpha\right). \tag{10b}$$

The proposed normalization (8) suggests that the scaling of the relative permeability in equation (10) is valid in the interval of saturations where the phases are mobile. Inspection of equation (10) leads to the following observations. The relative permeability of the wetting phase scales with the square of the mobile saturation, while k_{nw}^{*} depends on the mobile saturation, the viscosity ratio, and the flow regime parameter. It is worth emphasizing that the only fitting parameters are the endpoint relative permeabilities, β_w and β_{nw}, and the flow regime parameter α. Differently from other widely used correlations such as the Corey (Corey, 1954) and the Brooks-Corey (Brooks & Corey, 1964) relationships, the exponents of equation (10) are not fitting parameters but have been obtained as a result of homogenization theory based on flow regimes (Picchi & Battiato, 2018), and the postulation provided in equation (7).

In equation (10), the term $2\alpha MS_{*}/(1 - S_{*})$ represents a correction to the relative permeability that accounts for deviations from the CP flow scaling behavior. Such correction term vanishes in two regimes characterized by different underlying physical mechanisms, i.e., when $M \ll 1$ and/or $\alpha = 0$. While the low Ca number case (i.e., $\alpha \to 0$) corresponds to the "classical" CP configuration in Figure 1a, the $M \ll 1$ limit (e.g., gas-liquid systems) corresponds to any fluid configuration, dynamically equivalent to the CP, where the nonwetting phase sees the fluid-fluid interface as a solid wall and the relative permeability is just proportional to the square of the fluid saturation. Therefore, αM, i.e., the interplay between the viscosity ratio M and the capillary number Ca through the flow regime parameter α, can be used as a criterion to classify different dynamical behaviors. This leads to the definition of the following three classes:

- *Class I*: for $M \ll 1$, namely, $\mu_{nw} \ll \mu_w$, the capillary and viscous limits converge and both relative permeabilities scale with the square of saturation. The effect of the flow regime parameter (and the capillary number) is negligible, i.e.,

$$k_{w}^{*} \sim S_{*}^{2}, \qquad k_{nw}^{*} \sim \left(1 - S_{*}\right)^{2}. \tag{11}$$

- *Class II*: for viscosity ratios of order 1, $\mathcal{O}(M) = \mathcal{O}(1)$, in the capillary regime (quasi-static CP regime at very low Ca and $\alpha = 0$), both relative permeabilities scale with the square of saturation, i.e.,

$$k_{w}^{*} \sim S_{*}^{2}, \qquad k_{nw}^{*} \sim \left(1 - S_{*}\right)^{2}. \tag{12}$$

- *Class III*: for viscosity ratios of order 1, $\mathcal{O}(M) = \mathcal{O}(1)$, at intermediate and high Ca the effect of pore-scale flow regimes is always relevant and the relative permeabilities are defined by equation (10).

In the following section, we will derive an analytical expression for the fractional flow using the model for relative permeabilities presented above.

2.3. Regime-Specific Fractional Flow Equations

The macroscale equations presented in Picchi and Battiato (2018) include a conservation law for the saturation that, in the Darcy's limit, can be cast in terms of fractional flow, i.e.,

$$\frac{\partial S_w}{\partial t} + \langle \overline{\boldsymbol{u}} \rangle \cdot \nabla f_w = 0, \tag{13}$$

where $\langle \overline{\boldsymbol{u}} \rangle = \left\langle \overline{\boldsymbol{u}}_w \right\rangle + \left\langle \overline{\boldsymbol{u}}_{nw} \right\rangle$ is the total Darcy velocity and f_w is the fractional flow of the wetting phase defined as

$$f_w = \frac{q_w}{q_w + q_{nw}} = \frac{1}{1 + \frac{q_{nw}}{q_w}}, \tag{14}$$

with $q_w = A\left\langle \overline{\boldsymbol{u}}_w \right\rangle$ and $q_{nw} = A\left\langle \overline{\boldsymbol{u}}_{nw} \right\rangle$ the volumetric flow rates of the wetting and nonwetting phases, respectively, and A the cross-sectional area. Under the hypothesis that two-phase Darcy's law is valid, equations (1) and (14) can be combined to obtain

$$f_w = \frac{1}{1 + \frac{1}{M}\frac{k_{nw}}{k_w}}. \tag{15}$$

Inserting (10) into (15), one obtains an analytical expression for f_w, i.e.,

$$f_w = \frac{1}{1 + \beta^* \frac{(1-S_*)^2}{S_*^2}\left(\frac{1}{M} + \frac{2\alpha S_*}{1-S_*}\right)}, \tag{16}$$

where $\beta^* = \beta_{nw}/\beta_w$ is the ratio between the endpoint relative permeabilities of the nonwetting and wetting phase, respectively. Similarly, the fractional flow of the nonwetting phase is given by

$$f_{nw} = \frac{q_{nw}}{q_w + q_{nw}} = \frac{1}{1 + S_*^2\left[\beta^*\left(1 - S_*\right)^2\left(\frac{1}{M} + \frac{2\alpha S_*}{1-S_*}\right)\right]^{-1}}. \tag{17}$$

In this form, the expression for the fractional flows incorporates the effects of pore-scale flow regimes, with f_w and f_{nw} explicit functions of mobile saturation, viscosity ratio, endpoint relative permeabilities, and capillary number through the flow regime parameter, i.e., $f_w(S_*, M, \beta^*, Ca)$ and $f_{nw}(S_*, M, \beta^*, Ca)$. Equations (16) and (17) allow one to derive analytical expressions for the fractional flow and its derivatives, $\partial f/\partial S_w$, or its dimensionless counterpart $\partial f/\partial S_*$, in lieu of their numerical approximations, when upscaled equations are implemented in reservoir simulators. In Appendix A, the analytical expressions of the fractional flow derivatives are reported for completeness.

3. Discussion

In this section, we validate the model for the relative permeability, equation (10), with data available from the literature. First, we compare the model predictions with the pore-scale numerical simulations of Armstrong et al. (2016) and, then, with experiments. We also validate the fractional flow predictions.

3.1. Validation With Numerical Simulations

We use the set of numerical results of Armstrong et al. (2016) to validate the proposed $k^* - S_*$ model. In their work, pore-scale simulations of immiscible fluids (water and decane) were carried out on a real pore space geometry using a lattice Boltzmann method. Specifically, 3-D segmented images of a rock core were used to reconstruct the pore space geometry as well as the location of the fluid-fluid interface, used as the initial condition for the numerical simulations. Steady state simulations of fractional flow at a fixed saturation were carried out by imposing periodic boundary conditions and an external driving force, and the topology of the phases and the relative permeabilities were computed for a wide range of capillary number. The latter is a critical information needed to determine the flow regime parameter as a function of the capillary number. Based on the physical properties of water and decane, the viscosity ratio is of order one ($M = 0.9$) and, following the classification proposed in section 2.2, this set of data belongs to Class III.

Figure 2 shows the comparison between the predictions of the proposed model, equation (10), and the measured relative permeability of the wetting (Figures 2a and 2c) and nonwetting (Figures 2b and 2d) phases in linear (a and b) and semi–log (c and d) scales (log-log plots are provided in the insets); for this specific set of data $\beta_w = \beta_{nw} = 1$ and $S_* = S_w$, i.e., the model is fit free in the capillary limit when $\alpha = 0$ or has only α as a fitting parameter at intermediate values of Ca. Figure 2a (or 2c) shows that the relative permeability of the wetting phase, k_w, scales with the square of saturation, i.e.,, the trend derived by the model is captured. It is worth observing, though, that Figure 2a (or 2c) suggests that the relative permeability of the wetting phase depends on Ca (or α). In the proposed model, the flow regime parameter does not appear in (10a) due to the choice of the CAF as the viscous limiting case. A possibility to account for k_w dependence on α is the choice of the plug flow closures (section 4.4 in Picchi & Battiato, 2018) as the viscous limit. However, this choice would require the determination of an additional parameter, i.e., the film thickness, and, to the best of our knowledge, a model which correlates the film thickness and the capillary number for ganglia flow in a porous matrix has not been proposed yet. Figure 2b (or 2d) shows the predicted (lines) and measured (symbols) relative permeability of the nonwetting phase. Specifically, the experimental points (solid triangles), where the phases are assumed to be separated by a rigid partition, are here associated to the quasi-static CP flow regime. In this regime, i.e., in the capillary limit, when $\alpha = 0$ in equation (10b), there is a good agreement between data and model. It is worth emphasizing that this specific prediction is fit free. Solid circles in Figure 2b (or 2d) refer to simulations at intermediate values of Ca, where, as the capillary number increases, the nonwetting phase may either remain static or flow through the pore space in the form of ganglia. Also, in this scenario, the model predictions at $\alpha = const$ capture well the data trend. Furthermore, at a fixed saturation, k_{nw} saturates to a maximal relative permeability at high Ca, that is well described by the predicted viscous limit (equation (10b) with $\alpha = 1$).

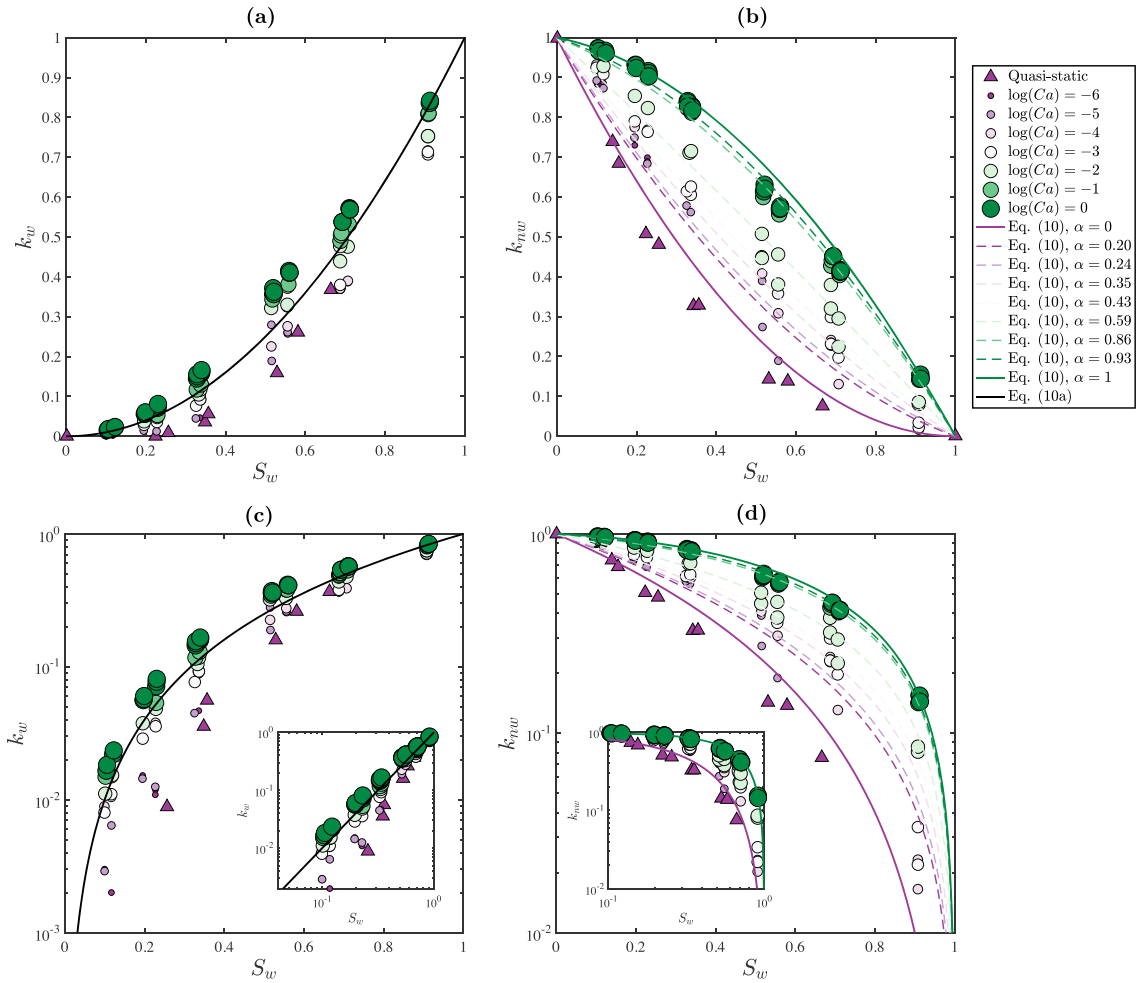

Figure 2. Validation of equation (8) against the pore-scale simulations of Armstrong et al. (2016): (a and c) relative permeability of the wetting phase in linear and semi–log scale, respectively; (b and d) relative permeability of the nonwetting phase in linear and semi–log scale, respectively. Loglog plots are in the insets. In all plots, solid lines represent the capillary (connected pathway) and viscous (viscous connected pathway) limits, while the dashed lines refer to intermediate *Ca* regimes (i.e., coexistence of ganglia and connected pathway).

The previous comparison suggests that the CP and VCP limiting curves may be interpreted as the lower and the upper bound of the relative permeability of the nonwetting phase, as summarized in the conceptualization sketch of Figure 1. Specifically, the VCP limit is obtained in analogy with the CAF in a capillary tube which represents the more efficient configuration in terms of transport of the nonwetting phase for viscosity ratio $M \geq 0.4$, as demonstrated by Picchi and Battiato (2018). This behavior is apparent also in realistic porous media, where *"high Ca flows lead to topological changes that support a more efficient transport at the Darcy scale"* (quote from Armstrong et al., 2016).

At intermediate *Ca*, predictions of k_{nw} require the determination of the flow regime parameter α. As shown in Figure 3, a fixed value of α fits well the relative permeabilities measured at a constant capillary number, thus supporting the hypothesis that the flow regime parameter is controlled by the capillary number and that the transition from the capillary to the viscous limits varies linearly with the percentage of the whole core occupied by each flow regime, see section 2.2. Similar conclusions can be drawn from the data set of Avraam and Payatakes (1995, 1999). Specifically, data fitting at constant *Ca* provides the following $\alpha - Ca$ correlation

$$\alpha = 0.13 \log(Ca) + 0.91, \quad \text{with} \quad 10^{-6} < Ca < 1, \tag{18}$$

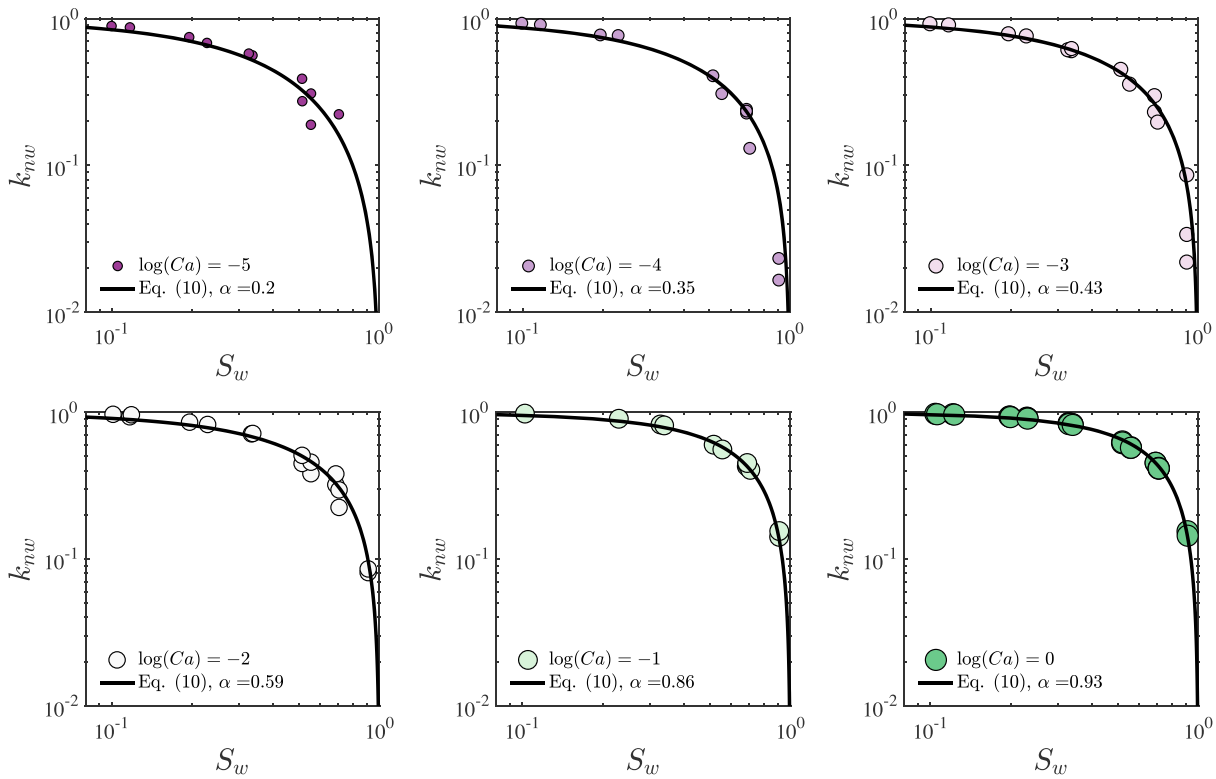

Figure 3. Determination of the flow regime parameter α as a function of the capillary number Ca: a fixed value of α fits well relative permeabilities measured at constant capillary numbers.

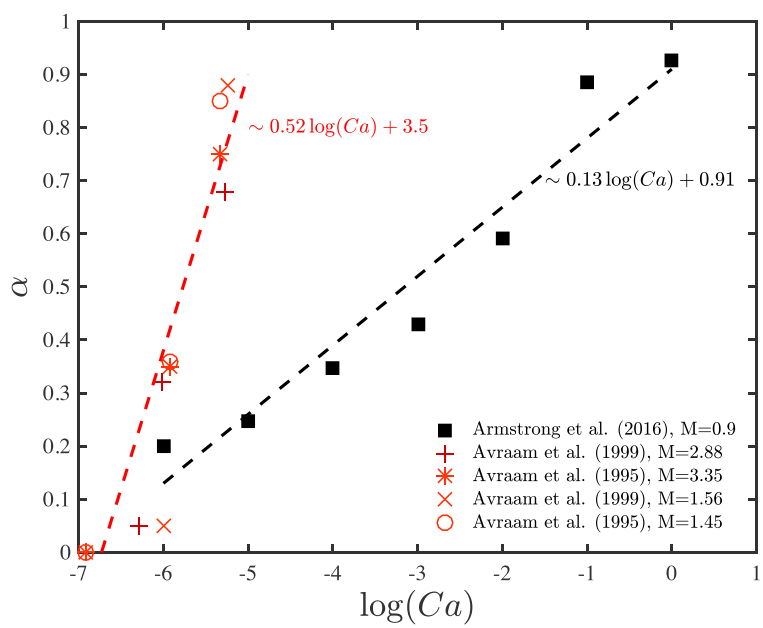

Figure 4. Flow regime parameter α as a function of the capillary number of the wetting phase for the data set of Armstrong et al. (2016) and Avraam and Payatakes (1995).

Table 1
Parameters of Equation (10) and Classification of the Experimental Data Used in the Validation of the Model

Reference	$w - nw$	dra./imb.	M	S_{ir}	$1 - S_{or}$	α	β_w	β_{nw}	R^2_α	$R^2_{\beta_w}$	$R^2_{\beta_{nw}}$
Class I											
Chen and DiCarlo (2016)	brine-CO_2	dra.	0.08	0.50	1	—	0.73	0.57	—	0.93	0.90
Reynolds and Krevor (2015)	brine-CO_2	dra.[a]	0.05–0.12	0.25	0.65	—	0.09	0.35	—	0.84	0.95
	brine-CO_2	dra.[b]	0.04–0.07	0.30	0.90	—	0.55	0.21	—	0.91	0.94
Alizadeh and Piri (2014)	oil-nitrogen	dra.	0.01	0.21	1	—	1.00	0.53	—	0.98	0.92
	oil-nitrogen	imb.	0.01	0.21	0.59	—	0.12	0.67	—	0.98	0.95
	water-nitrogen	dra.	0.02	0.23	1	—	0.93	0.43	—	0.97	0.95
	water-nitrogen	imb.	0.02	0.23	0.62	—	0.13	0.56	—	0.97	0.97
Manceau et al. (2015)	brine-CO_2	dra.	0.08	0.50	0.73	—	0.01	0.08	—	0.82	0.91
	brine-CO_2	imb.	0.08	0.50	0.73	—	0.10	0.08	—	0.95	0.99
Perrin and Benson (2010)	brine-CO_2	dra.	0.08	0.44	0.87	—	0.49	0.48	—	0.92	0.92
Pini and Benson (2013)	water-gCO_2	dra.	0.03	0.40	0.90	—	—	0.56	—	—	0.96
	water-scCO_2	dra.	0.03	0.40	0.75	—	—	0.71	—	—	0.97
	water-nitrogen	dra.	0.04	0.40	0.75	—	—	0.67	—	—	0.70
Ruprecht et al. (2014)	water-CO_2	imb.	0.04	0.50	0.87	—	0.33	0.71	—	0.95	0.43
	water-CO_2	imb.	0.04	0.50	0.80	—	0.21	0.32	—	0.98	0.52
	water-CO_2	imb.	0.04	0.50	0.75	—	0.16	0.33	—	0.99	0.99
	water-CO_2	dra.	0.04	0.50	1	—	0.62	0.12	—	0.98	0.86
Class II											
Armstrong et al. (2016)	water-decane	dra.[c]	0.90	0	1	0	1	1	—	0.96	0.96
Berg et al. (2016)	brine-ndecane	imb.	0.90	0.21	0.62	0	0.06	0.55	—	0.99	0.97
	brine-ndecane	imb.[c]	0.90	0.21	0.71	0	0.34	0.55	—	0.96	0.99
Gao et al. (2017)	brine-decane	dra.[d]	0.90	0.21	0.62	0	0.06	0.55	—	0.90	0.99
Class III											
Armstrong et al. (2016)	water-decane	dra.[c]	0.90	0	1	0.2–0.9	1	1	0.99	0.96	0.99
Gao et al. (2017)	brine-decane	dra.[d]	0.90	0.21	0.62	0.16	0.06	0.55	0.93	0.76	0.93
Avraam and Payatakes (1995)	water-nHexadecane	imb.	3.35	0.30	0.66	0–0.75	0.10	0.30	0.90	—	0.90
Avraam and Payatakes (1995)	water-nDodecane	imb.	1.45	0.10	0.68	0–0.85	0.10	0.40	0.95	—	0.95
Avraam and Payatakes (1999)	Formamide-nNonanol	imb.	2.88	0.10	0.70	0–0.68	0.25	0.80	0.95	0.75	0.95
Avraam and Payatakes (1999)	water-nDodecane	imb.	1.56	0.10	0.60	0–0.88	0.16	0.20	0.80	—	0.80

Note. The coefficient of determination R^2 for the three fitting parameters β_w, β_{nw}, and α is also calculated.
[a]Viscous limit. [b]Capillary limit. [c]Numerical experiments. [d]Low Ca data.

where Ca is the capillary number of the wetting phase, defined in equation (5). Although this relation (see Figure 4) is specific to the set of data analyzed here, it suggests that the flow regime parameter α is not a purely fitting parameter, but it is connected to the pore-scale physics.

To sum up, we have validated the proposed model against numerical simulations, see Figure 2, and proposed guidelines to correlate the flow regime parameter α to the capillary number Ca. In the following, an overall validation is presented where model predictions are compared against data collected in experiments performed on 3-D rock samples at different capillary numbers and viscosity ratios.

3.2. Validation With Experimental Data

In this section we validate the scaling relationship against experimental data available in the literature. The data were selected such that two-phase relative permeabilities measurements were available as well as information on both the flow regimes and the capillary number: this knowledge is necessary to test the predictions of the $k^* - S_*$, equation (10). The overall set of data analyzed includes 410 experiments either in the capillary or in the viscous regime and spans 2 orders of magnitude in viscosity ratio, with M in the range $M = 0.01 \div 3$, as summarized in Table 1. The validation has been carried out following the procedure described below.

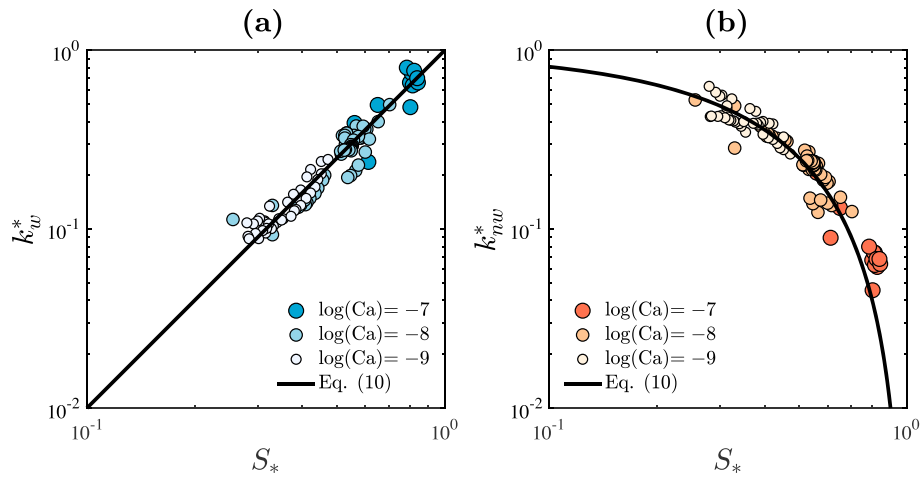

Figure 5. Comparison between the predicted and experimentally measured (Chen & DiCarlo, 2016) rescaled relative permeability as a function of the mobilized saturation. The viscosity ratio of the system (brine-CO_2) is M= 0.08, while the capillary number is defined by equation (5), where the velocity scale is defined by the ratio of the volumetric flow rate to the cross-section area of the core sample.

3.2.1. Data Analysis Procedure

This analysis aims at obtaining the rescaled relative permeability k_w^* and k_{nw}^*, defined by equation (8), in terms of mobile saturation, S_*, defined by equation (9), for all the data sets listed in Table 1. The data are processed as follows:

1. We identify whether the experimental data set belongs to Class I, Class II, or Class III depending on the viscosity ratio.
2. We identify whether the experiments exhibit residual and irreducible saturations, S_{ir}, and S_{or}.
3. We rescale the saturations of the wetting phase in terms of mobile saturation.
4. If the data set belongs to Class I and Class II, we fit the endpoint saturations β_w and β_{nw}; if the data set belongs to Class III, we fit the endpoint relative permeabilities and we also look for the dependence of the parameter α with the capillary number.

All the details on the classification of the data set used are provided in Table 1, including references, values of the fitting parameters, and the estimation of the error of the model obtained from our analysis.

3.2.2. Class I

As previously discussed, Class I is characterized by a small viscosity ratio ($M \ll 1$), i.e., the nonwetting phase is much less viscous than the wetting phase, $\mu_{nw} \ll \mu_w$, such as in brine-CO_2 and water-nitrogen systems, and the effects of the pore-scale flow regimes are negligible. As a result, the capillary and viscous limits converge to the same curve. This behavior is confirmed by the data of Chen and DiCarlo (2016) reported in Figure 5: although the relative permeabilities were measured at three different capillary numbers (spanning three orders of magnitude), the data are not "stratified" with respect to the capillary number and instead lay on the same universal curve, well described by the scaling relationship (11), i.e., the normalized relative permeability scales with the square of the mobile saturation.

Furthermore, we tested the scaling (11) against other sets of experimental data both at imbibition and drainage conditions (Alizadeh & Piri, 2014; Manceau et al., 2015; Perrin & Benson, 2010; Pini & Benson, 2013; Ruprecht et al., 2014; Reynolds & Krevor, 2015), and the overall comparison is shown in Figure 6; Table 1 contains the full set of model parameters as well as the coefficient of determination for the fitted parameters. The data collapse around the scaling (11) for the whole range of saturations both in linear and logarithmic scales. This suggests that equation (11) captures the trend displayed by the data for systems belonging to Class I: some of the variability is indeed expected due to the semiempirical nature of the model and the intrinsic nature of multiphase flow experiments (see Ling et al., 2017). The trend is captured also when the effect of rock heterogeneity is taken into account: in the experiments of Reynolds and Krevor (2015) for the same test fluids, the heterogeneity in the rock sample affects the residual and irreducible saturation and endpoint relative permeability, but does not change the overall scaling behavior of the $k^* - S_*$ relationships.

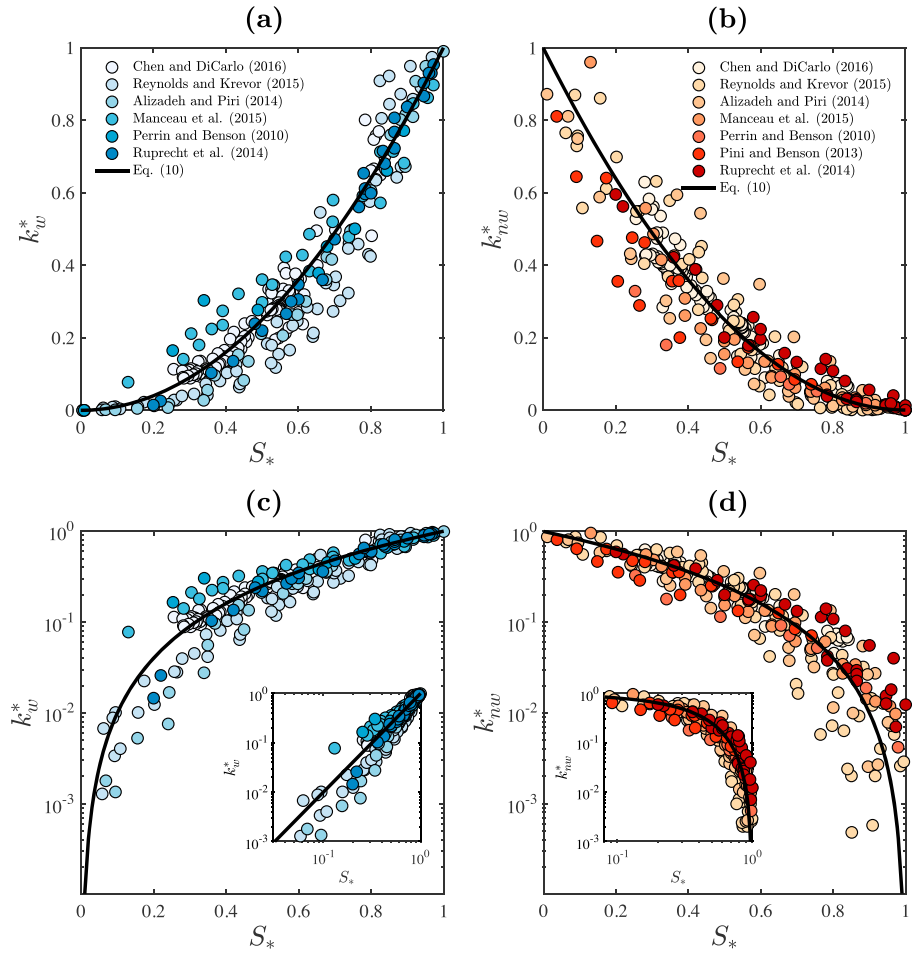

Figure 6. Class I data comparison: Comparison between the predicted scaling of the normalized relative permeability of the wetting (a and c) and nonwetting (b and d) phases in terms of the mobile saturation and Class I experimental measurements from real core samples available in the literature. (a) and (b) plots are in linear scale, while (c) and (d) plots are in semi–log scale. Log-log plots are available in the insets.

3.2.3. Class II

Flow systems in Class II are characterized by a viscosity ratio of order 1 and flow conditions in the capillary regime. Figure 7 shows that the normalized relative permeabilities follow the trend predicted by equation (12) for the experimental data of Armstrong et al. (2016), Berg et al. (2016), and Gao et al. (2017). Concerning the data of Gao et al. (2017), we refer to the experiments performed at the lowest capillary number where no intermittency of the nonwetting phase has been observed. It is worth emphasizing that, despite the scaling of Class II systems is the same as that of Class I, in the former the dominant flow regime is the quasi-static CP flow, see Figure 1a; this behavior is accounted for by setting $\alpha = 0$.

3.2.4. Class III

Relative permeabilities in different flow regimes have been measured in a few studies only. Among them, we compare our model with the data by Avraam and Payatakes (1995, 1999). In these studies, experiments were conducted at steady state flow conditions: at intermediate Ca, the authors observe the coexistence of ganglion flow dynamics and CP flow, while, at higher Ca, the flow is dominated by VCPs. Furthermore, the experimental observation that a lubricating thin layer of wetting phase wets the pore walls supports the model CAF analogy, at least for relatively simple systems as those considered by Avraam and Payatakes (1995, 1999), see Figure 1c. The overall validation of k_{nw}^* is presented in Figures 8a–8d, where, in addition to the endpoint relative permeabilities, the flow regime parameter α was used as a fitting parameter to model all experimental points at a constant capillary number. The model predictions given by equation (10b) can capture the experimental data trend as well as the change in steepness of the $k^* - S_*$ curves between low and high Ca.

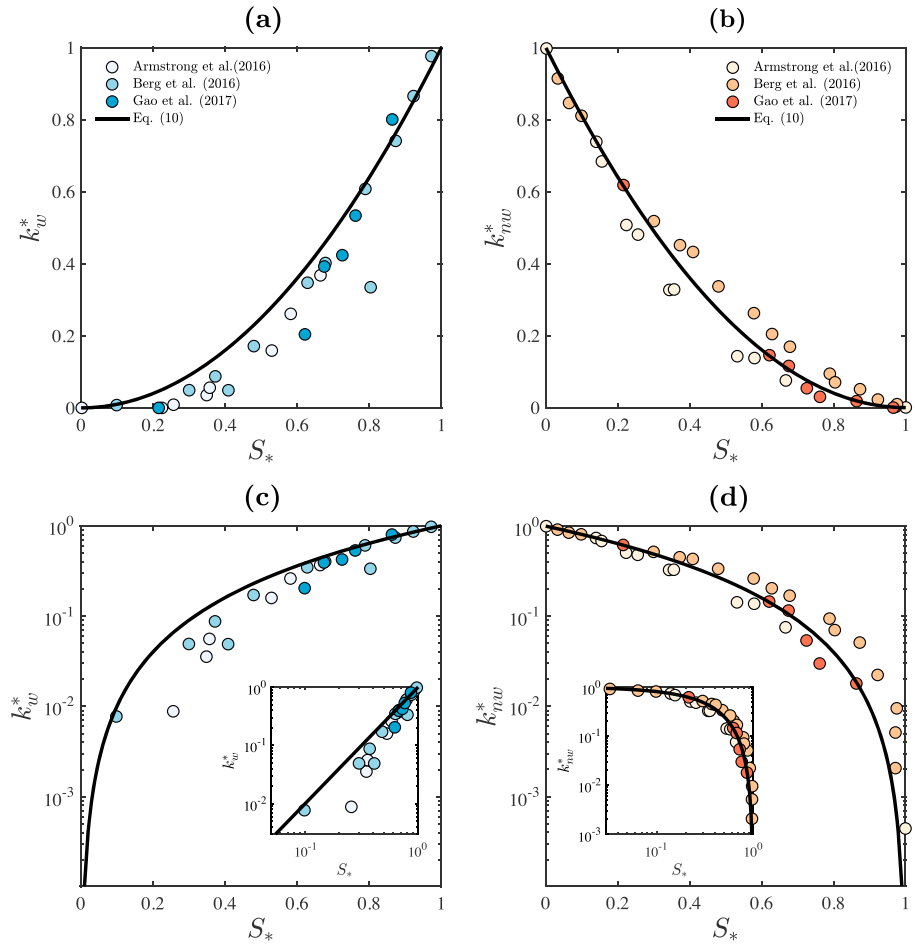

Figure 7. Class II data comparison: comparison between the predicted scaling of the normalized relative permeability of the wetting (a and c) and nonwetting (b and d) phase in terms of the mobile saturation and Class II experimental measurements from real core samples available in the literature. (a) and (b) plots are in linear scale, while (c) and (d) plots are in semi–log scale. Log-log plots are available in the insets.

For this set of data, the flow regime parameter is plotted as a function of the capillary number in Figure 4:

$$\alpha = 0.52 \log(Ca) + 3.5 \quad \text{with} \quad 10^{-6.7} < Ca < 10^{-5}. \tag{19}$$

The difference between (18) and (19) may be due to a number of factors: (i) the relation between the flow regime parameter and the capillary number is strongly influenced by the type of core sample used and (ii) the capillary number has been defined and computed differently by Avraam & Payatakes (1995, 1999) and Armstrong et al. (2016). As a result, we are not able to verify whether the $\alpha - Ca$ data may or may not exhibit a universality behavior, although Figure 4 does suggest the existence of a more general relation, since α depends linearly to the logarithm of Ca in both the cases shown. Yet, the possibility of finding a general scaling for the flow regime parameter remains an open question.

Figure 8e shows that the relative permeability of the wetting phase scales with the square of the mobile saturation, even though the data present more variability compared to the cases of Class I and Class II. Finally, in Figure 8f we show a comparison with the data collected by Gao et al. (2017), where data points at higher Ca start to the deviate from the quasi-static CP flow curve, and the trends are well captured by the model.

3.3. Fractional Flow

In this section we compare the analytical expressions derived for the fractional flow curves, equations (16) and (17), with experimental measurements.

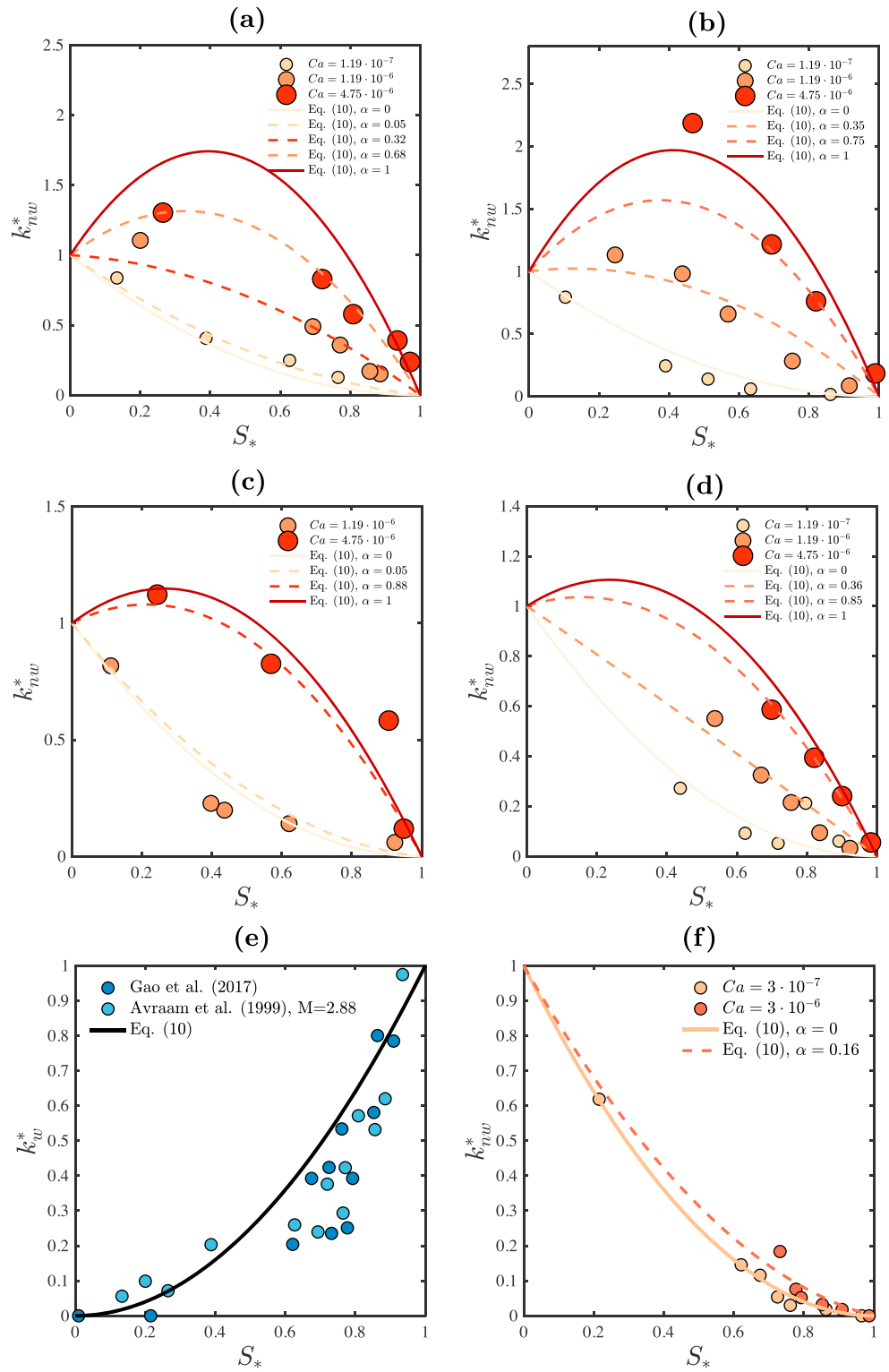

Figure 8. Class III data comparison: comparison between the predicted scaling of the normalized relative permeability in terms of the mobile saturation and Class III experimental measurements from real core samples available in the literature. (a) Avraam and Payatakes (1999), $M = 2.88$; (b) Avraam and Payatakes (1995), $M = 3.35$; (c) Avraam and Payatakes (1999), $M = 1.56$; (d) Avraam and Payatakes (1995), $M = 1.45$; (e) wetting phase; (f) Gao et al. (2017), $M = 0.9$.

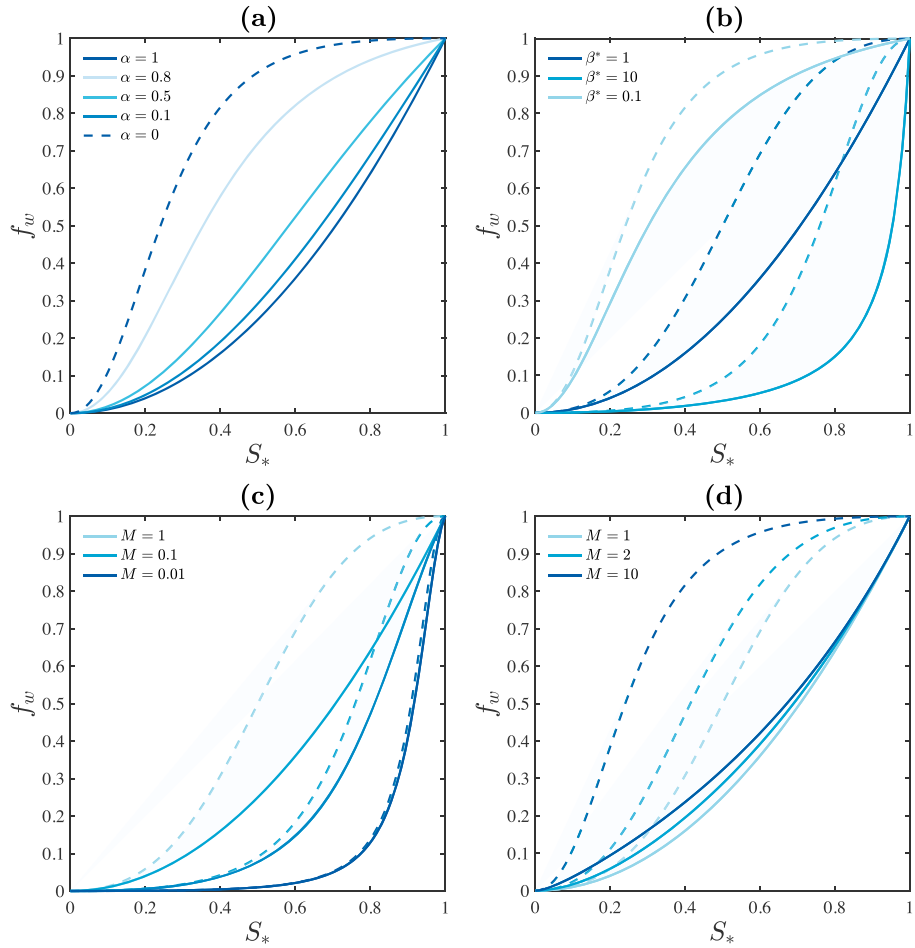

Figure 9. Sensitivity of the fractional flow curve of the wetting phase with respect to the governing parameters: (a) the flow regime parameter α at $M = 1$, $\beta^* = 1$; (b) the ratio of the endpoints relative permeability $\beta^* = \beta_{nw}/\beta_w$ at $M = 1$; and (c and d) the viscosity ratio M at $\beta^* = 1$. Dashed curves and solid lines represent $\alpha = 0$ and $\alpha = 1$, respectively.

In Figure 9a we show the sensitivity of the fractional flow of the wetting phase to the flow regime parameter for the case of isoviscous fluids: in the capillary regime ($\alpha = 0$), f_w has a typical s-shape, while the curve becomes increasingly concave as $\alpha \to 1$, that is, moving to the viscous regime ($\alpha = 1$). As shown in section 3, the flow regime parameter can be expressed as a function of the capillary number, and therefore, the fractional flow computed at a fixed value of the flow regime parameter describes systems at a constant capillary number. Figure 9b shows the effect of β^* on the fractional flow: the dashed lines represent the capillary limit, the solid lines the viscous limit, while the solid-colored region identifies the transition for α between 0 and 1. Specifically, for $\beta^* < 1$, the fractional flow shrinks to a s-shape curve, while, for $\beta^* > 1$, the slope changes and the transition region (the colored region) gets wider. Figures 9c and 9d show the effect of the viscosity ratio: for $M \to 0$, $f_w \to 0$ and the capillary and viscous regime curves coincide, while, for $M > 1$, the transition region becomes much wider.

Once the normalized relative permeabilities are obtained as described in section 3.2, fractional flow predictions are a free outcome of the model and do not require any additional fitting parameter. In Figure 10a we show the comparison with the data from Reynolds and Krevor (2015): not only the analytical profile matches the data well, but the s-shape trend typical of Class I data is well reproduced. Furthermore, the predicted trends of the derivative of f_{nw} relative to the mobile saturation are shown in Figure 10b for the three cases presented (each curve corresponds to different viscosity ratios and β^*, see Table 1).

Finally, in Figure 10c we report a comparison against the data by Avraam and Payatakes (1999). Despite the agreement is not as satisfactory as previous comparisons, the overall trends are captured with the experi-

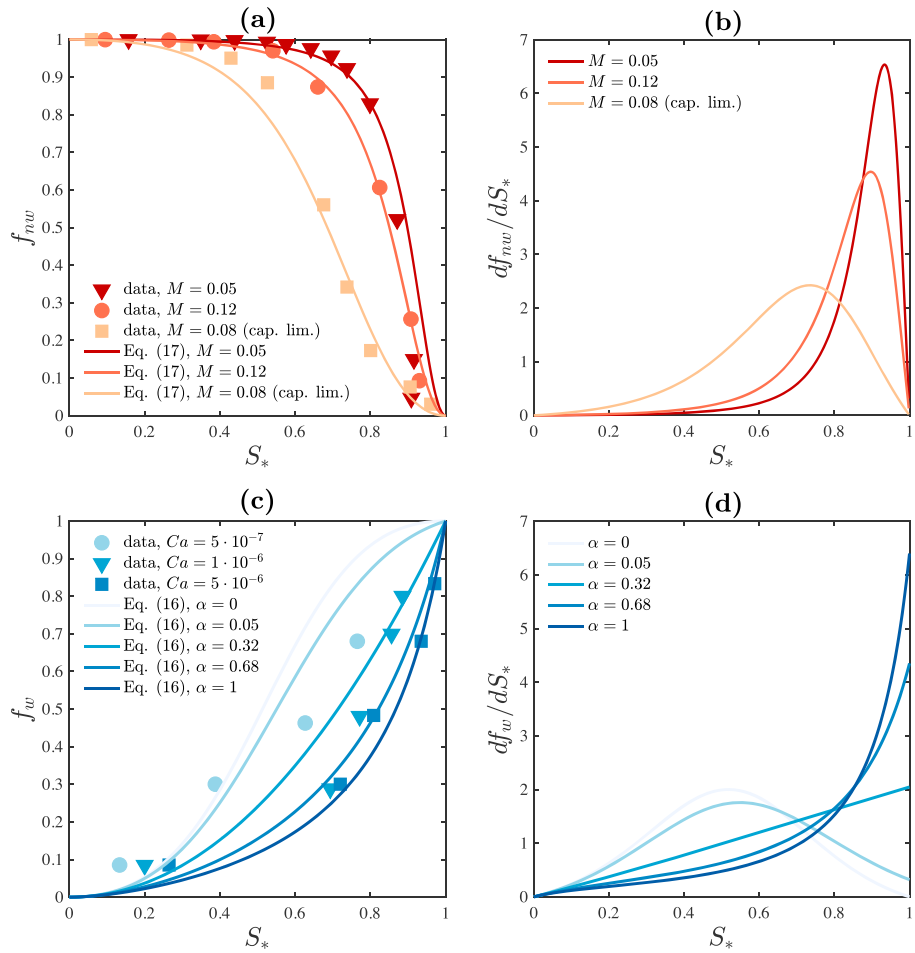

Figure 10. Comparison between the predicted fractional flow curve in terms of the mobile saturation with experimental data of (a) Reynolds and Krevor (2015), Class I, nonwetting phase and (c) Avraam and Payatakes (1999), Class III, $M = 2.88$, wetting phase. The derivatives of the fractional flow curves are also presented in (b) and (d), respectively.

mental points laying in the region within the capillary and viscous limits. This may be due to the additional complexity of the phase topology for systems belonging to Class III.

4. Conclusions

In this work, we proposed a semiempirical model for relative permeabilities that accounts for pore-scale flow regimes and it includes both the capillary and viscous limits. The model well captures the scaling structure of the relative permeability: the rescaled relative permeability of the wetting phase depends only on the mobile saturation, while the relative permeability of the nonwetting phase is a function of the mobile saturation, the viscosity ratio, and the capillary number. The model contains three fitting parameters, i.e., the two endpoint relative permeabilities and the flow regime parameter, although when the viscosity ratio is sufficiently small, the fitting parameters reduce to two, since the effect of the flow regime parameter—or the capillary number—becomes negligible. The major conclusions of this study are summarized below:

1. We identify three classes of systems depending on the viscosity ratio. Systems with a small viscosity ratio (i.e., the wetting phase is much more viscous than the nonwetting phase) belong to Class I: in this regime, both relative permeabilities scale as the square of the fluid saturation. Systems with a viscosity ratio of order 1 in the capillary regime (i.e., low capillary number) belong to Class II: similarly to the previous case, both relative permeabilities scale as the square of the fluid saturation. Systems with a viscosity ratio of order 1 and where pore-scale flow regimes are observed at intermediate capillary number belong to

Class III: in this case, the relative permeability of the nonwetting phase is a function also of the viscosity ratio and the capillary number through the flow regime parameter.

2. The proposed model is able to capture the trend of the relative permeability measurements in complex 3-D porous rocks for all three classes.
3. We derived an analytical expression for the fractional flow, and we validated it against experimental measurements. The slope of the fractional curve changes with the capillary number for Class III systems, while approaching the viscous regime (i.e., high capillary number).

Notwithstanding research effort is still needed to address many open questions, for example, the developments of a model to systematically predict the endpoint relative permeability and residual and irreducible saturations, we believe that the proposed model is a promising starting point to correlate pore-scale flow regimes and effective parameters at the continuum scale.

Appendix A: Fractional Flow Derivatives

In this appendix we provide the analytical expression of the partial derivative of the fractional flow of the wetting and the nonwetting phase relative to the mobile saturation:

$$\frac{\partial f_w}{\partial S_*} = -\frac{\partial f_{nw}}{\partial S_*} = -\frac{2\beta^* M S_* \left(M S_* \alpha S_* - 2M\alpha S_* + S_* - 1\right)}{\left(-2M S_* \beta^* \alpha S_* + M S_*^2 + 2M\beta^* \alpha S_* + S_*^2 \beta^* - 2S_* \beta^* + \beta^*\right)^2}. \tag{A1a}$$

The derivative with respect to the saturation of the wetting phase is easily recovered from

$$\frac{\partial f_w}{\partial S_w} = \frac{\partial f_w}{\partial S_*} \frac{1}{1 - S_{ir} - S_{or}}. \tag{A2}$$

Acknowledgments
Full support by the Department of Energy under the Early Career Award DE-SC0014227 "Multiscale dynamics of reactive fronts in the subsurface" is gratefully acknowledged. The paper is theoretical, and no data are used. We would like to thank Ryan Armstrong (University of New South Wales) and James E. McClure (Virginia Polytechnic Institute and State University) for sharing the data of their simulations.

References

Alizadeh, A. H., & Piri, M. (2014). The effect of saturation history on three-phase relative permeability: An experimental study. *Water Resources Research*, *50*, 1636–1664. https://doi.org/10.1002/2013WR014914

Armstrong, R. T., McClure, J. E., Berrill, M. A., Rücker, M., Schlüter, S., & Berg, S. (2016). Beyond Darcy's law: The role of phase topology and ganglion dynamics for two-fluid flow. *Physical Review E*, *94*, 043113. https://doi.org/10.1103/PhysRevE.94.043113

Armstrong, R. T., Ott, H., Georgiadis, A., Rucker, M., Schwing, A., & Berg, S. (2014). Subsecond pore-scale displacement processes and relaxation dynamics in multiphase flow. *Water Resources Research*, *50*, 9162–9176. https://doi.org/10.1002/2014WR015858

Armstrong, R. T., Porter, M. L., & Wildenschild, D. (2012). Linking pore-scale interfacial curvature to column-scale capillary pressure. *Advances in Water Resources*, *46*, 55–62. https://doi.org/10.1016/j.advwatres.2012.05.009

Arunachalam, H., Onori, S., & Battiato, I. (2015). On veracity of macroscopic lithium-ion battery models. *Journal of the Electrochemical Society*, *162*(10), A1940–A1951.

Auriault, J.-L. (1987). Nonsaturated deformable porous media: Quasistatics. *Transport in Porous Media*, *2*(1), 45–64. https://doi.org/10.1007/BF0020853

Avraam, D. G., & Payatakes, A. C. (1995). Flow regimes and relative permeabilities during steady-state two-phase flow in porous media. *Journal of Fluid Mechanics*, *293*, 207–236.

Avraam, D. G., & Payatakes, A. C. (1999). Flow mechanisms, relative permeabilities, and coupling effects in steady-state two-phase flow through porous media. The case of strong wettability. *Industrial & Engineering Chemistry Research*, *38*(3), 778–786. https://doi.org/10.1021/ie980404o

Bear, J. (1972). *Dynamics of fluids in porous media*, Dover Civil and Mechanical Engineering Series. Dover: New York: American Elsevier Publishing Company.

Berg, S., Ott, H., Klapp, S. A., Schwing, A., Neiteler, R., Brussee, N., et al. (2013). Real-time 3D imaging of haines jumps in porous media flow. *Proceedings of the National Academy of Sciences*, *110*(10), 3755–3759. https://doi.org/10.1073/pnas.1221373110

Berg, S., Rucker, M., Ott, H., Georgiadis, A., van der Linde, H., Enzmann, F., et al. (2016). Connected pathway relative permeability from pore-scale imaging of imbibition. *Advances in Water Resources*, *90*, 24–35.

Blunt, M. J., Bijeljic, B., dong, H., Gharbi, O., Iglauer, S., Mostaghimi, P., et al. (2013). Pore-scale imaging and modelling. *Advances in Water Resources*, *51*, 197–216.

Brooks, R. H., & Corey, A. T. (1964). Hydraulic properties of porous media. *Hydrology Papers*, *3*, 1–29.

Chen, X., & DiCarlo, D. A. (2016). A new unsteady-state method of determining two-phase relative permeability illustrated by CO_2-brine primary drainage in Berea sandstone. *Advances in Water Resources*, *96*, 251–265.

Chierici, G. L. (1984). Novel relations for drainage and imbibition relative permeabilities. *Society of Petroleum Engineers Journal*, *24*(03), 275–276. https://doi.org/10.2118/10165-PA

Clavier, R., Chikhi, N., Fichot, F., & Quintard, M. (2017). Modeling of inertial multi-phase flows through high permeability porous media: Friction closure laws. *International Journal of Multiphase Flow*, *91*, 243–261.

Corey, A. T. (1954). The interrelation between gas and oil relative permeabilities. *Producers Monthly*, *19*, 38–41.

Cueto-Felgueroso, L., & Juanes, R. (2012). Macroscopic phase-field model of partial wetting: Bubbles in a capillary tube. *Physical Review Letters*, *108*(144), 502. https://doi.org/10.1103/PhysRevLett.108.144502

Cueto-Felgueroso, L., & Juanes, R. (2014). A phase-field model of two-phase hele-shaw? flow. *Journal of Fluid Mechanics*, *758*, 522–552.

Daly, K. R., & Roose, T. (2015). Homogenization of two fluid flow in porous media, Proceedings of the Royal Society of London A: Mathematical. *Physical and Engineering Sciences*, *471*(2176). https://doi.org/10.1098/rspa.2014.0564

Datta, S. S., Dupin, J.-B., & Weitz, D. A. (2014). Fluid breakup during simultaneous two-phase flow through a three-dimensional porous medium. *Physics of Fluids*, *26*(6), 062004. https://doi.org/10.1063/1.4884955

Dehghanpour, H., Aminzadeh, B., Mirzaei, M., & DiCarlo, D. A. (2011). Flow coupling during three-phase gravity drainage. *Physical Review E*, *83*, 065302. https://doi.org/10.1103/PhysRevE.83.065302

Gao, Y., Lin, Q., Bijeljic, B., & Blunt, M. J. (2017). X-ray microtomography of intermittency in multiphase flow at steady state using a differential imaging method. *Water Resources Research*, *53*, 10,274–10,292. https://doi.org/10.1002/2017WR021736

Garing, C., de Chalendar, J. A., Voltolini, M., Ajo-Franklin, J. B., & Benson, S. M. (2017). Pore-scale capillary pressure analysis using multi-scale X-ray micromotography. *Advances in Water Resources*, *104*, 223–241. https://doi.org/10.1016/j.advwatres.2017.04.006

Gray, W. G., Dye, A. L., McClure, J. E., Pyrak-Nolte, L. J., & Miller, C. T. (2015). On the dynamics and kinematics of two-fluid-phase flow in porous media. *Water Resources Research*, *51*, 5365–5381. https://doi.org/10.1002/2015WR016921

Gray, W. G., & Miller, C. T. (2010). Thermodynamically constrained averaging theory approach for modeling flow and transport phenomena in porous medium systems: 8. Interface and common curve dynamics. *Advances in Water Resources*, *33*(12), 1427–1443.

Gunstensen, A. K., & Rothman, D. H. (1993). Lattice-Boltzmann studies of immiscible two-phase flow through porous media. *Journal of Geophysical Research*, *98*(B4), 6431–6441. https://doi.org/10.1029/92JB02660

Hassanizadeh, M., & Gray, W. G. (1980). General conservation equations for multi-phase systems: 3. Constitutive theory for porous media flow. *Advances in Water Resources*, *3*(1), 25–40. https://doi.org/10.1016/0309-1708(80)90016-0

Hassanizadeh, S. M., & Gray, W. G. (1990). Mechanics and thermodynamics of multiphase flow in porous media including interphase boundaries. *Advances in Water Resources*, *13*(4), 169–186.

Hassanizadeh, S. M., & Gray, W. G. (1993). Toward an improved description of the physics of two-phase flow. *Advances in Water Resources*, *16*(1), 53–67.

Hilfer, R. (1998). Macroscopic equations of motion for two-phase flow in porous media. *Physical Review E*, *58*, 2090–2096. https://doi.org/10.1103/PhysRevE.58.2090

Hornung, U. (1997). *Homogenization and porous media*. New York NY: Springer-Verlag New York, Inc.

Jackson, S. J., Agada, S., Reynolds, C. A., & Krevor, S. (2018). Characterizing drainage multiphase flow in heterogeneous sandstones. *Water Resources Research*, *54*, 3139–3161. https://doi.org/10.1029/2017WR022282

Jackson, A. S., Miller, C. T., & Gray, W. G. (2009). Thermodynamically constrained averaging theory approach for modeling flow and transport phenomena in porous medium systems: 6. Two-fluid-phase flow. *Advances in Water Resources*, *32*(6), 779–795.

Karadimitriou, N. K., Hassanizadeh, S. M., Joekar-Niasar, V., & Kleingeld, P. J. (2014). Micromodel study of two-phase flow under transient conditions: Quantifying effects of specific interfacial area. *Water Resources Research*, *50*, 8125–8140. https://doi.org/10.1002/2014WR015388

Kjelstrup, S., Bedeaux, D., Hansen, A., Hafskjold, B., & Galteland, O. (2018). Non-isothermal transport of multi-phase fluids in porous media. The entropy production. *Frontiers in Physics*, *6*, 126. https://doi.org/10.3389/fphy.2018.00126

Lake, L. W. (1989). *Enhanced oil recovery*. NJ: Prentice Hall: Prentice Hall. Englewood Cliffs.

Lasseux, D., Ahmadi, A., & Arani, A. A. A. (2008). Two-phase inertial flow in homogeneous porous media: A theoretical derivation of a macroscopic model. *Transport in Porous Media*, *75*(3), 371–400. https://doi.org/10.1007/s11242-008-9231-y

Leverett, M. C. (1941). Capillary behavior in porous solids. *Society of Petroleum Engineers*, *142*, 152–169.

Li, J., Chen, Z., Wu, K., Li, R., Xu, J., Liu, Q., et al. (2018). Effect of water saturation on gas slippage in tight rocks. *Fuel*, *225*, 519–532.

Li, Z., Galindo-Torres, S., Yan, G., Scheuermann, A., & Li, L. (2018b). A lattice Boltzmann investigation of steady-state fluid distribution, capillary pressure and relative permeability of a porous medium: Effects of fluid and geometrical properties. *Advances in Water Resources*, *116*, 153–166. https://doi.org/10.1016/j.advwatres.2018.04.009

Li, H., Pan, C., & Miller, C. T. (2005). Pore-scale investigation of viscous coupling effects for two-phase flow in porous media. *Physical Review E*, *72*(026), 705. https://doi.org/10.1103/PhysRevE.72.026705

Lin, Q., Bijeljic, B., Pini, R., Blunt, M. J., & Krevor, S. (2018). Imaging and measurement of pore-scale interfacial curvature to determine capillary pressure simultaneously with relative permeability. *Water Resources Research*, *54*, 7046–7060. https://doi.org/10.1029/2018WR023214

Ling, B., Bao, J., Oostrom, M., Battiato, I., & A. M. Tartakovsky, A. M. (2017). Modeling variability in porescale multiphase flow experiments. *Advances in Water Resources*, *105*, 29–38.

Manceau, J. C., Ma, J., Li, R., Audigane, P., Jiang, P. X., Xu, R. N., et al. (2015). Two-phase flow properties of a sandstone rock for the CO_2/water system: Core-flooding experiments, and focus on impacts of mineralogical changes. *Water Resources Research*, *51*, 2885–2900. https://doi.org/10.1002/2014WR015725

McClure, J. E., Armstrong, R. T., Berrill, M. A., Schlüter, S., Berg, S., Gray, W. G., & Miller, C. T. (2018). Geometric state function for two-fluid flow in porous media. *Physical Review Fluids*, *3*, 084306. https://doi.org/10.1103/PhysRevFluids.3.084306

McClure, J. E., Berrill, M. A., Gray, W. G., & Miller, C. T. (2016). Influence of phase connectivity on the relationship among capillary pressure, fluid saturation, and interfacial area in two-fluid-phase porous medium systems. *Physical Review E*, *94*, 033102. https://doi.org/10.1103/PhysRevE.94.033102

Niessner, J., & Hassanizadeh, S. M. (2008). A model for two-phase flow in porous media including fluid-fluid interfacial area. *Water Resources Research*, *44*, W08439. https://doi.org/10.1029/2007WR006721

Oliveira, L. I., & Demond, A. H. (2003). Estimation of primary drainage three-phase relative permeability for organic liquid transport in the vadose zone. *Journal of Contaminant Hydrology*, *66*(3), 261–285.

Perrin, J.-C., & Benson, S. (2010). An experimental study on the influence of sub-core scale heterogeneities on CO_2 distribution in reservoir rocks. *Transport in Porous Media*, *82*(1), 93–109. https://doi.org/10.1007/s11242-009-9426-x

Picchi, D., & Battiato, I. (2018). The impact of pore-scale flow regimes on upscaling of immiscible two-phase flow in porous media. *Water Resources Research*, *54*, 6683–6707. https://doi.org/10.1029/2018WR023172

Picchi, D., Poesio, P., Ullmann, A., & Brauner, N. (2017). Characteristics of stratified flows of Newtonian/non-Newtonian shear-thinning fluids. *International Journal of Multiphase Flow*, *97*, 109–133. https://doi.org/10.1016/j.ijmultiphaseflow.2017.06.005

Pasquier, S., Quintard, M., & Davit, Y. (2017). Modeling two-phase flow of immiscible fluids in porous media: Buckley-leverett theory with explicit coupling terms. *Physical Review Fluids*, *2*, 104101. https://doi.org/10.1103/PhysRevFluids.2.104101

Picchi, D., Ullmann, A., & Brauner, N. (2018). Modeling of core-annular and plug flows of newtonian/non-newtonian shear-thinning fluids in pipes and capillary tubes. *International Journal of Multiphase Flow*, *103*, 43–60. https://doi.org/10.1016/j.ijmultiphaseflow.2018.01.023

Pini, R., & Benson, S. M. (2013). Simultaneous determination of capillary pressure and relative permeability curves from core-flooding experiments with various fluid pairs. *Water Resources Research*, *49*, 3516–3530. https://doi.org/10.1002/wrcr.20274

Prodanovic, M., Lindquist, W., & Seright, R. (2006). Porous structure and fluid partitioning in polyethylene cores from 3D X-ray microtomographic imaging. *Journal of Colloid and Interface Science*, *298*(1), 282–297. https://doi.org/10.1016/j.jcis.2005.11.053

Prodanovic, M., Lindquist, W. B., & Seright, R. S. (2007). 3D image-based characterization of fluid displacement in a Berea core. *Advances in Water Resources*, *30*, 214–226.

Reynolds, C. A., & Krevor, S. (2015). Characterizing flow behavior for gas injection: Relative permeability of CO_2-brine and N_2-water in heterogeneous rocks. *Water Resources Research*, *51*, 9464–9489. https://doi.org/10.1002/2015WR018046

Reynolds, C. A., Menke, H., Andrew, M., Blunt, M. J., & Krevor, S. (2017). Dynamic fluid connectivity during steady-state multiphase flow in a sandstone. *Proceedings of the National Academy of Sciences*, *114*(31), 8187–8192. https://doi.org/10.1073/pnas.1702834114

Rucker, M., Berg, S., Armstrong, R. T., Georgiadis, A., Ott, H., Schwing, A., et al. (2015). From connected pathway flow to ganglion dynamics. *Geophysical Research Letters*, *42*, 3888–3894. https://doi.org/10.1002/2015GL064007

Ruprecht, C., Pini, R., Falta, R., Benson, S., & Murdoch, L. (2014). Hysteretic trapping and relative permeability of CO_2 in sandstone at reservoir conditions. *International Journal of Greenhouse Gas Control*, *27*, 15–27.

Rybak, I. V., Gray, W. G., & Miller, C. T. (2015). Modeling two-fluid-phase flow and species transport in porous media. *Journal of Hydrology*, *521*, 565–581.

Schluter, S., Berg, S., Rucker, M., Armstrong, R. T., Vogel, H.-J., Hilfer, R., & Wildenschild, D. (2016). Pore-scale displacement mechanisms as a source of hysteresis for two-phase flow in porous media. *Water Resources Research*, *52*, 2194–2205. https://doi.org/10.1002/2015WR018254

Tahmasebi, P., Sahimi, M., Kohanpur, A. H., & Valocchi, A. (2017). Pore-scale simulation of flow of CO_2 and brine in reconstructed and actual 3D rock cores energy Frontier Research Centers for Investigating Carbon Sequestration. *Journal of Petroleum Science and Engineering*, *155*, 21–33. https://doi.org/10.1016/j.petrol.2016.12.031

Tallakstad, K. T., Løvoll, G., Knudsen, H. A., Ramstad, T., Flekkøy, E. G., & Måløy, K. J. (2009). Steady-state, simultaneous two-phase flow in porous media: An experimental study. *Physical Review E*, *80*(036), 308. https://doi.org/10.1103/PhysRevE.80.036308

Ullmann, A., & Brauner, N. (2004). Closure relations for the shear stresses in two-fluid models for core-annular flow. *Multiphase Science and Technology*, *16*(4), 355–387.

Whitaker, S. (1986). Flow in porous media II: The governing equations for immiscible, two-phase flow. *Transport in Porous Media*, *1*(2), 105–125. https://doi.org/10.1007/BF00714688

Yang, H., Xu, Z., Fan, M., Gupta, R., Slimane, R. B., Bland, A. E., & Wright, I. (2008). Progress in carbon dioxide separation and capture: A review. *Journal of Environmental Sciences*, *20*(1), 14–27.

Yiotis, A. G., Psihogios, J., Kainourgiakis, M. E., Papaioannou, A., & Stubos, A. K. (2007). A lattice boltzmann study of viscous coupling effects in immiscible two-phase flow in porous media. *Colloids and Surfaces A: Physicochemical and Engineering Aspects*, *300*(1), 35–49. Proceedings of the Fourth International TRI/Princeton Workshop Characterization of Porous Materials: from Angstroms to Millimeters.

Zarikos, I., Terzis, A., Hassanizadeh, S. M., & Weigand, B. (2018). Velocity distributions in trapped and mobilized non-wetting phase ganglia in porous media. *Scientific Reports*, *8*(1), 13228. https://doi.org/10.1038/s41598-018-31639-4

Zhang, T., Li, X., Li, J., Feng, D., Wu, K., Shi, J., et al. (2018). A fractal model for gas–water relative permeability in inorganic shale with nanoscale pores. *Transport in Porous Media*, *122*(2), 305–331. https://doi.org/10.1007/s11242-018-1006-5